

See discussions, stats, and author profiles for this publication at: <https://www.researchgate.net/publication/268470528>

# Modelling and Simulation of a Novel Dual Axes Tilt Quadrotor UAV

Conference Paper · August 2013

DOI: 10.2514/6.2013-4595

---

CITATIONS

11

READS

1,787

5 authors, including:



Pau Segui-Gasco

Cranfield University

8 PUBLICATIONS 228 CITATIONS

[SEE PROFILE](#)



Hyo-Sang Shin

Korea Advanced Institute of Science and Technology

315 PUBLICATIONS 4,047 CITATIONS

[SEE PROFILE](#)

# Modelling and Simulation of a Novel Dual Axes Tilt Quadrotor UAV

Yazan Al-Rihani,\*

*KADDB, Amman, Jordan*

Pau Segui-Gasco†, Hyo-Sang Shin‡, Al Savvaris § and Francis Salama ¶

*Cranfield University, Cranfield, Bedfordshire, MK43 0AL, United Kingdom*

This paper presents the design and modelling of a novel multi rotor actuation approach. In order to increase the agility and reliability of the multi-rotors, the novel concept seeks to fuse 3 main actuation mechanisms, namely, gyroscopic torques, thrust vectoring and differential thrusting. The design of a novel quadrotor implementing the Dual Axes Tilting concept is presented. A detailed modelling of the new actuator suite, which includes the development of the gyroscopic equations for the propellers, the characterisation of the propeller aerodynamics and the dynamic identification of both the motors and the servomotors, is described. Finally, the results of the simulation model are compared with those of the real vehicle by conducting experiments on a test rig. On the light of the results it can be stated that the simulation model is representative of the dynamics of the real vehicle.

## I. Introduction

Inexpensive small Unmanned Aerial Vehicles (UAVs) have considerable potential for use in many aspects. They are cheaper and more versatile than manned vehicles, and are ideally suited for dangerous, long and/or monotonous missions that would be inadvisable or impossible for a human pilot. The large scale of small UAVs applications has thus proliferated vastly within the last few years<sup>13</sup>. Among many other types of UAVs, quadrotors are widely used in research and development because they are simple, easy to operate and maintain when compared with other vehicles.

Quadrotors have its own problems, namely, there are two major issues, reliability and agility. If any of actuators fails, the vehicle is completely de-stabilised due to its dependence on the symmetry of the lift. In order to mitigate this reliability issue, two approaches have been proposed in our previous study:<sup>12</sup> the first approach uses propellers with a variable pitch and the second approach shifts the CG. Although both of the proposed approaches could reconfigure the controllability in pitch and roll axes, the yaw axis remained uncontrollable. Agility is also another issue in multi-rotor because they don't scale up well. As a multi-rotor scales up there are two main problems that slow down its dynamic response. First, as shown by<sup>13</sup> as the vehicle scales up its inertia builds up demanding much larger control moments to create the same angular acceleration on the airframe. Second, as the weight builds up, assuming a constant disc loading, the propellers inertia scales with the square of the vehicle weight, thus, making the change of its angular velocity much slower as the size of the vehicle increases, and hence, reducing the control bandwidth. This is a physical boundary that the conventional quadrotor has in its performance. As the weight increases the bandwidth of the actuation dramatically decreases.

\*Researcher, King Abdullah Design and Development Bureau (KADDB), Amman, Jordan

†PhD Student, Department of Engineering Physics. AIAA Student Member.

‡Lecturer, Department of Engineering Physics, AIAA Member.

§Lecturer, Department of Engineering Physics.

¶Researcher, Department of Engineering Physics.

The main objective of this study is to develop a novel actuation architecture that overcomes the two main problems of conventional quadrotors, control bandwidth and reliability, and validate the proposed architecture. One naive approach to solve some of the issues that affect a conventional quadrotor is to increase the number of rotors, usually, to six rotors, hexarotoros, or eight, octorotors. This approach has several advantages among them are mechanical simplicity, it increases the number of actuators and hence, is reliability is increased. However this approach might fail to increase the agility, i.e. the bandwidth, because the number of propellers must grow matching the increase in weight, to keep the bandwidth high, but this could imply a possibly unacceptably large number of propellers for moderate weights.

Other strategies involve a variety of actuation devices. As usual with aircraft design key constraints that must be considered are its size and weight. A very effective approach has been shown by Cutler et al<sup>5</sup> using propellers with variable pitch, in their approach while the authors manage to keep the weight down they increase the bandwidth of its actuators, and so, of the vehicle. However at a cost of a more complex propeller and servomotor system to drive the pitch variation.

Efforts to increase the bandwidth of the actuators of the control system have been conducted using Control Moment Gyroscopes (CMG), the same way as spacecraft govern their attitude, see.<sup>11</sup> In this work the authors merge a thrust vectoring approach with increased bandwidth including additional flywheels to use as CMG. This approach however greatly complicates the system and increases its weight because the aircraft needs to carry the extra weight of the flywheels and the thrust vectoring vane system.

Gary R. Gress<sup>7</sup> came up with the idea of using Opposed Lateral Tilting as a means of using the gyroscopic effects for governing the pitch attitude of his aircraft, using the propellers as gyroscopes. His latest work<sup>8</sup> provides an overview of the Oposed Lateral Tilting (OLT) philosophy. In this work, the author provides, through a simplified modelling, evidence of the feasibility of the gyroscopic actuation for governing pitch attitude. In<sup>8</sup> OLT is proved to give higher control authority than other means of actuation such as vaned fans. In an independent work<sup>9</sup> the authors conducted a more detailed modelling of a platform based on the OLT strategy and provide evidence of the effectivity of this technique in simulation. Later the same group<sup>1</sup> put these concepts into practice into the vehicle T-Phoenix UAV, providing a detailed model and a control strategy for hovering, showing experimental evidence of the feasibility of the OLT strategy. In the work<sup>14</sup> the authors provide also a survey of OLT technology and a more in depth modelling of the tilting phenomena allowing for distinct angular velocities and tilt angles of the two thrusters.

Our proposed novel concept of actuation, see,<sup>15</sup> is the utilisation of dual axis tilting which exploits three different actuation types: gyroscopic, thrust vectoring and differential thrusting are fused into one concept by using a dual axes tilting propeller system. Gyroscopic torques are achieved by using the angular momentum and fast tilting of its rotational axes. Thrust vectoring is achieved by orienting the thrust of each propeller independently of the body. Differential thrusting is achieved by the conventional quadrotor strategy of differential angular velocities in the rotors. To achieve all this 3 actuation principles a new multi-rotor arm concept has been developed.

In order to explore the feasibility of this concept the strategy followed has considered the following steps, first, a novel arm concept has been developed, second, a realisation of this concept has been designed using Commercial Off-The-Shelf (COTS) materials to produce a prototype quadrotor, third, a mathematical model has been developed of all the relevant actuation phenomena, fourth, based on this model a conventional control system has been designed to stabilise the vehicle and finally the vehicle has been flight tested. All this process is described in our paper.<sup>15</sup> In this paper a more in depth description of the vehicle design and a more detailed analysis of the modelling and simulation of this novel platform is developed.

The main contribution of this paper is, then, the design description and the modelling and simulation of the vehicle. The model of the new actuators is composed of 3 main aspects, gyroscopic torques modelling, propeller characterisation and motor dynamic identification. The simulation model is arranged around the well known 6DOF equations of motion with the addition of the aforementioned 3 main actuation effects. Finally a series of tests are conducted to validate the simulation model with the comparison of the prediction and the experimental results on a test rig.

This paper is structured as follows. First a description of the actuation concept and the vehicle is carried out. Second, the main actuation effects of the system are described and the simulation model arrangement is explained. Third, the control system of the vehicle is briefly described. Fourth, a brief comparison of the simulation model with experimental results from a rig test is conducted. And finally a discussion of the results is presented.

## II. Vehicle Design

### A. Tilting Mechanism

A realisation of this novel arm concept is shown in figure 1. Here we have used commercially available parts to minimise the number of custom manufactured parts. This design is based around the servoblock<sup>16</sup> part, which is a standard size servo holder aluminum brackets designed specially to increase the servo capability to carry lateral loads by transferring the load to holding structure. It has one small bearing on the front bracket. The servoblock serves as a frame to mount a standard size RC servo which allows it to move the whole arm around its axis. On the arm there is another servo mounted which is connected through a pushpull mechanism to the motor mount which swivels parallel to the servo lever. Thus, the propeller rotational axis can be freely configured with the two angles generated by the servomotors. Henceforth, this two angles/motions will be named servoblock and push-pull.

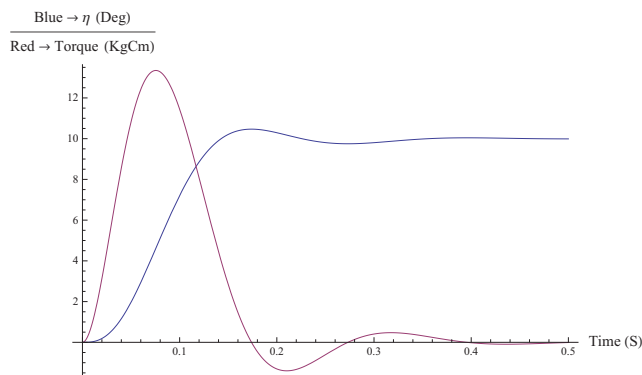


Figure 1. Tilting arm concept

Selecting the proper RC servo depends on three main things, torque, speed and size. Regarding the speed, the faster the better, because larger gyroscopic torques will be attained, and the size is constrained to a standard size RC servo because of the use of servoblocks. Regarding the torque, since one of the actuation principles is the gyroscopic torque and this effect happens in an axis orthogonal to the deflection, when one servo is tilted the other must stand the reaction torque of its counterpart. To estimate the amount of torque needed, a simulation was set up with the rigid body equations derived in the modelling section. With the propeller running at nominal speed a step demand on the servomotor was simulated and the torque in the orthogonal axis was recorded alongside the position of the deflecting servo. The model of the servo used in the simulation is based on a model of a standard size Hitech HSR-5990GT servo developed by Wada and others.<sup>18</sup> The results of the simulation, see figure 2, show that the gyroscopic reaction could reach 13 KgCm.

Searching on the market among Hitec and Futaba RC standard size servos; servoblocks are designed to work with those brands only; the Hitec servo HS-7940TH was selected, because it was the fastest servo capable of handling the desired torque with a safety margin. Table 1 shows the technical data for this servo.

To design the propellers of the vehicle it must be kept in mind that they exert a dual role, on one side they are thrusters, but on the other side they are flywheels. Hence, a compromise must be found between the two roles. Designing a propeller from scratch that would yield a good tradeoff between this two roles is a challenge that, certainly, would prove very fruitful, however, in the early stages of the conception, it was



**Figure 2.** Servo gyroscopic reaction

**Table 1.** Hitec servo HS-7940TH technical data

Specifications	7.4V
Speed	0.06 $\frac{s}{60^\circ}$
Torque	16.0 $\frac{kg}{cm}$

thought of it as a further refinement that would better be exploited once a first prototype has been flown and a deeper understanding had been earned. Hence, the problem became to find a suitable commercially available propeller that meet the needs.

The design task then, turned into a selection task. Which was to find a propeller with good inertia characteristics that, at the same time, provided the desired thrust characteristics. A 3 blade propeller was fundamental because otherwise large vibrations would arise from the inertia asymmetry in a 2 blade design. This is better illustrated in figure 3, where a simulation of the tilting torques compares a two blade vs a three blade propeller being tilt. Here, it can be clearly seen the vibrations arising from the two blade propeller assymetry.

Among the commercially available propellers, assuming a nominal weight of 3Kg of the vehicle, the Master Airscrew 3 blade 12x6 inch propeller was selected. Then, based on data from previous tests with equivalent propellers the motors selected to drive this propellers were the brushless DC outrunners MK3638 by Mikrokopter, powered by a the ESC Roxy Bl Control 930-6 from Robbe.

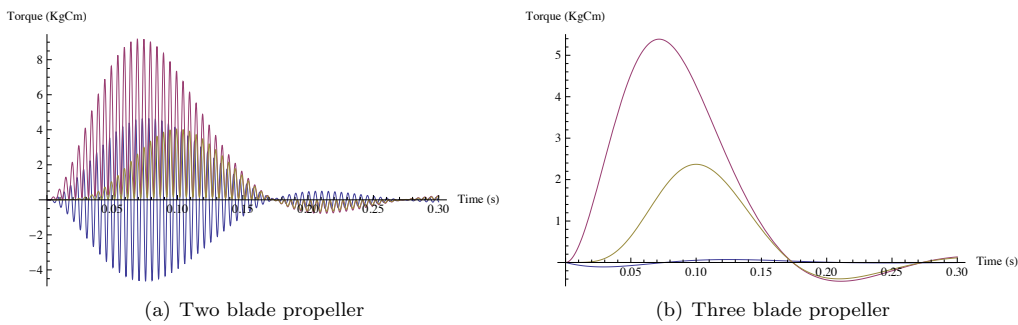


**Figure 3.** Two blade propellers compared to three blade propellers in tilting rotors

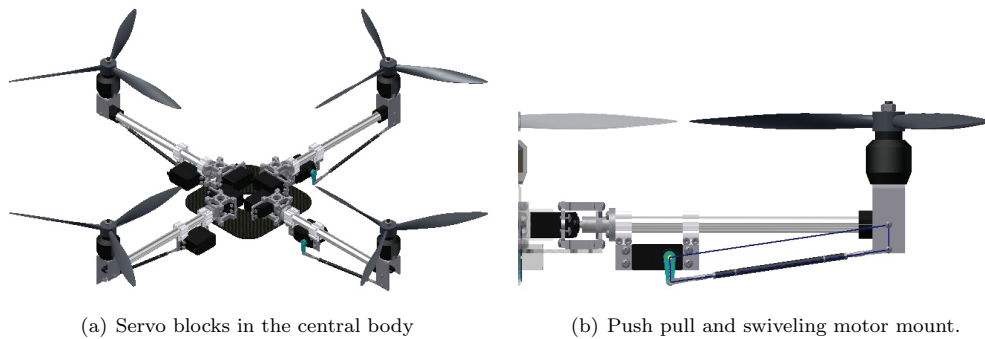


**Figure 4. Tilting mechanism**

## B. Overall Design

Putting it all together the arrangement of the servoblocks was carried out by fixing them to a carbon fibre plate which functioned as a central body, this can be seen in figure 4(a). The arm is a 0.5" diameter hollow 7075-T6 aluminium tube, which is fixed to the servoblock adapter using a 0.770" aluminium tube clamping hub, and by using another clamping hub, the pushpull servo was mounted as shown in figure 4(b).

Once the conceptual design of frame was clear a detail design of all the components was carried out in a CAD software. This included all the electronics and batteries, in figure 6(a) the 3D model is presented and the plans of the design with the key dimensions shown in figure 5. Finally, the mass properties of the vehicle were obtained from the CAD software and are specified in table 2. With everything specified, the prototype was built and it is shown in figure 6(b).

**Table 2. Mass and Inertia obtained from CAD.**

Mass	I <sub>xx</sub>	I <sub>yy</sub>	I <sub>zz</sub>	I <sub>xy</sub>	I <sub>xz</sub>	I <sub>yz</sub>
2.968 Kg	49827 kg mm <sup>2</sup>	48993 kg mm <sup>2</sup>	82777 kg mm <sup>2</sup>	12 kg mm <sup>2</sup>	35 kg mm <sup>2</sup>	295 kg mm <sup>2</sup>

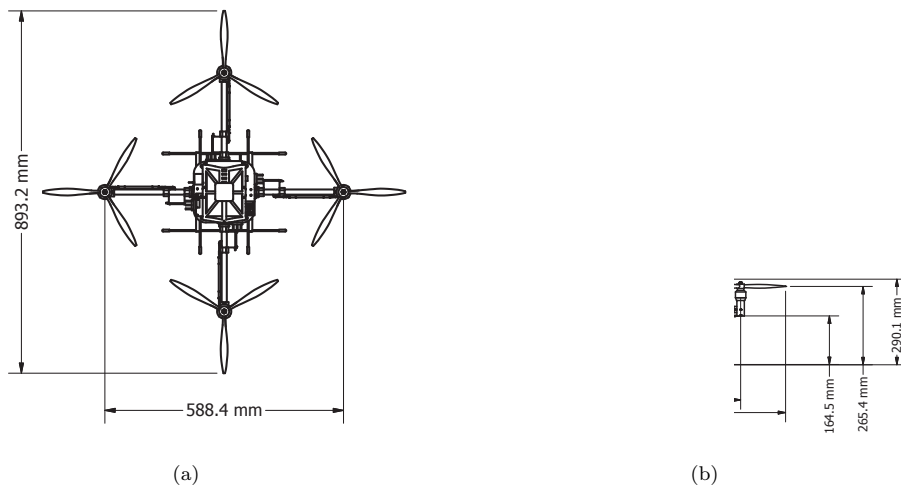


**Figure 5. Platform technical drawing**

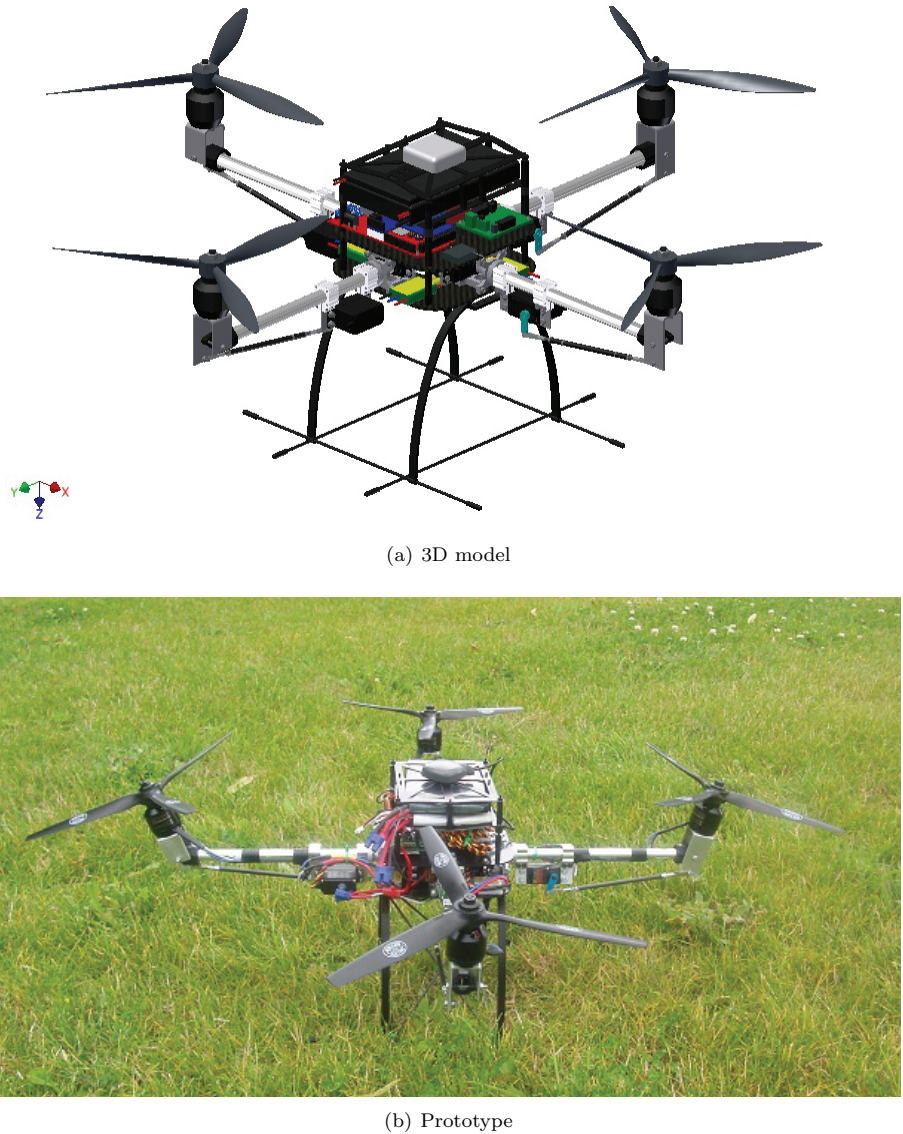


**Figure 6.** Dual axis Tilt rotor UAV

### C. Vehicle Systems.

There are three main systems on the vehicle, the power system, the control system and the communications system. The power system is composed of two batteries, one to power the servomotors, a LiPo 7.4V 2S1P 3200mAh 25C and another one to power the motors, a LiPo 14.8V 4S1P 5000mAh 20C. The control system is composed of three main parts, the sensors, the processor board and the servo/ESC driver board. The sensors are a an IMU by SBG Systems, the IG-500N, this unit has an embedded processor able to output filtered attitude and position data up to a 100 Hz. The processing board is a chipKit Max32 by Digilent that computes the control signal and the communications signals. And the servo/ESC driver board is a Parallax Propeller that reads a serial message from the MAX32 and issues the PWM signals for each of the 12 actuators. The communications system has two main components, the data telemetry and the command signal. The data telemetry is implemented using XBee modules by Digi. And the command signal is communicated using a Spektrum satellite receiver and a DX6i RC transmitter on the ground. All those systems were implemented in the electronics bay pictured in figure 7.

For further details on the design of the vehicle and the system the interested reader is pointed to the theses by Al-Rihani<sup>2</sup> and Segui-Gasco<sup>6</sup> where everything is further explained.

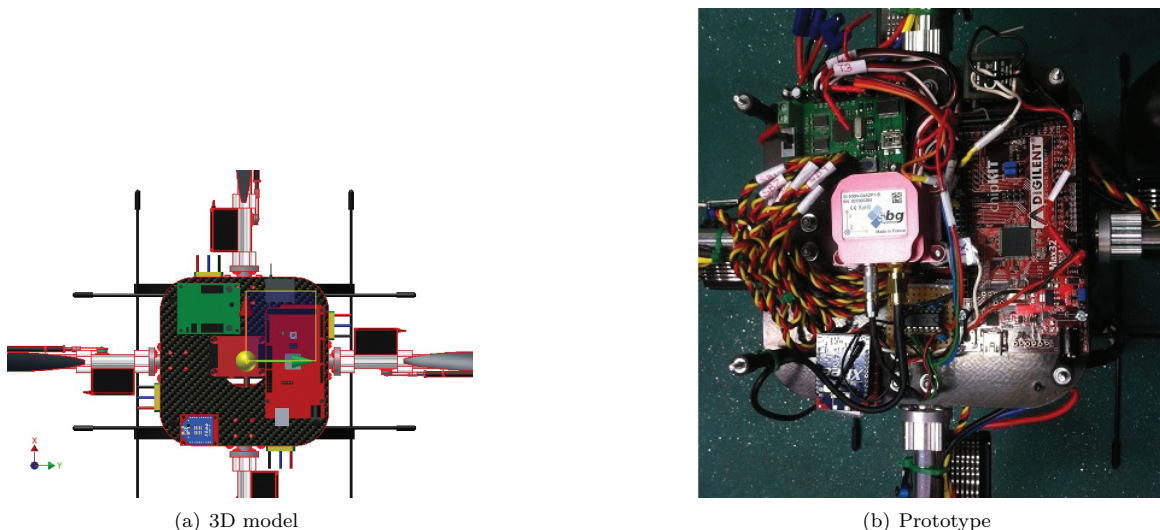


**Figure 7. Electronics layout**

### III. Control System Design

The vehicle, by its nature, is open loop unstable, so a control system must be designed in order to stabilise it. The objective of the first control system designed for this vehicle was, then, to implement a Stability Augmentation Control System (SCAS) for the attitude, such that, the pilot would issue commands from the transmitter of roll, pitch and yaw for the control system to track. The design of the control system was thought in a way that it would be simple to tune, efficient to implement and such that it took advantage of the over actuation present in this system. The architecture chosen was a PD loop for each axes and a Control Allocator. This is a classical approach in the design of control systems for air vehicles and has several known advantages, among others: ease of tuning, allowance to accommodate actuator failures and allowance to choose the actuator combination to optimise some cost function, e.g. minimising drag, actuator deflection or energy consumed.

The strategy was, then, to design a controller based on a control law that issued 3 virtual control commands, roll, pitch and yawing moments and a control allocator that translated those 3 moments and the desired overall thrust into individual control inputs for each of the 12 actuators. This way, the aforementioned objectives were obtained because the control allocator would create an abstraction layer in the design

process in a way that for the design of the control laws only 3 “virtual actuators” would have to be considered, instead of dealing with 12 different coupled individual actuators.

The design of the control law is based on a simple 3 SISO PD controllers, one for each axes feeding back the angle and the angular rate from the IMU to track the commanded Euler angles from the transmitter. The control allocator design was based on a linearisation of the control actions exerted by each actuator and a weighted pseudoinverse. Although this approach did not exploit the full potential of the actuator suite due to its linearity limitations, it provided an efficient and pragmatic implementation that reasonably fulfilled the need, while at the same time it was fast to execute on the microcontroller. The tuning and the design process of both are further explained in the theses by Al-Rihani<sup>2</sup> and Segui-Gasco,<sup>6</sup> and in the paper by Segui-Gasco, Al-Rihani et al.<sup>15</sup>

## IV. Model Development

### A. Introduction

In this section all the relevant actuations phenomena are analysed in order to produce a simulation model of the vehicle. The modelling of the actuation phenomena has 3 main parts. One is the development of the rigid body relations of the tilting propeller that describe the torque as a function of the vehicle motion and the tilting motions. Another is the characterisation of the propellers in terms of thrust and torque coefficients, and finally the individual actuators that create the tilting motion, servomotors, and the motors that vary the propeller’s angular speed are dynamically characterised. All this actions are then used in combination of the equations of motion of the vehicle to produce its simulation model. Then, all this phenomena and relations are structured in a simulation model that is described at the end of this section.

### B. Gyroscopic Effects Modelling

The gyroscopic effects are modelled as the reactions generated by individual rotors spinning due to the vehicle motion and tilt motion. In other words, it is assumed that each of the rotor-propeller assembly, shown in figure 8(a), does the job of a flywheel that, when tilted creates the gyroscopic torques.

The relations between the motion of the rotor  $j$  and the moments applied onto it expressed on the reference frame  $i$  airframe are given by the Euler equation:

$${}^i\mathbf{M}_j = {}^i\mathbf{I}_j {}^i\boldsymbol{\alpha}_j + {}^i\boldsymbol{\omega}_j \times {}^i\mathbf{I}_j {}^i\boldsymbol{\omega}_j \quad (1)$$

where  ${}^i\mathbf{M}_j$  is the moment in the centre of gravity of the rotor  $j$  expressed in reference frame  $i$ ,  ${}^i\mathbf{I}_j$  is the inertia tensor about the CG in the reference frame  $i$ ,  ${}^i\boldsymbol{\omega}_j$  is the total angular velocity of the body  $j$  and  ${}^i\boldsymbol{\alpha}_j$  is the total angular acceleration of the body  $j$  in the reference frame  $i$ , i.e.  ${}^i\boldsymbol{\alpha}_j = \frac{d}{dt} {}^i\boldsymbol{\omega}_j$ .

As can be inferred from figure 8(b) the vehicle presents symmetry both around the x-z plane and the y-z plane. Hence, the development of the equations is the for all four arms is actually the same if the reference frame is adequately transformed. For this reason, here, only the equations with respect to arm 3 will be developed and then, the equations regarding the remaining arms can be obtained by an appropriate frame change. Herein, arm 3 will be referred as standard arm or arm 3 indifferently.

#### 1. Reference Frames

Three non inertial reference frames are used to describe the rotating motion of the spinning assembly. These are illustrated in figure 9.

- Reference Frame 1 ( $x_1, y_1, z_1$ ) attached to the vehicle frame. With unit vectors  $\mathbf{i}_1 \mathbf{j}_1 \mathbf{k}_1$ .
- Reference Frame 2 ( $x_2, y_2, z_2$ ) attached to the Servoblock, i.e. to the arm. With unit vectors  $\mathbf{i}_2 \mathbf{j}_2 \mathbf{k}_2$ .
- Reference Frame 3 ( $x_3, y_3, z_3$ ) attached to the motor stator, i.e. parallel to the Pushpull lever and the motor swivelling bracket. With unit vectors  $\mathbf{i}_3 \mathbf{j}_3 \mathbf{k}_3$ .

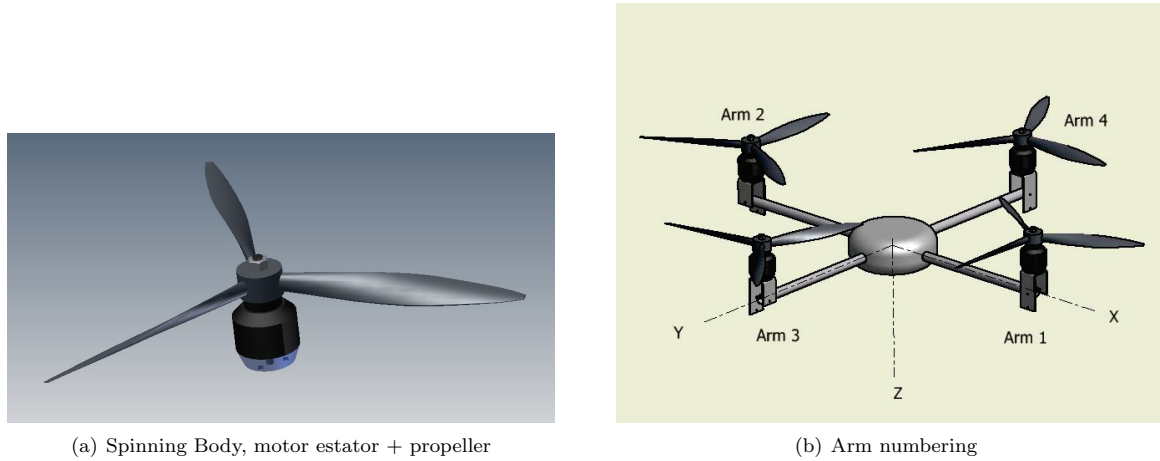


Figure 8. Spinning body and arm numbering illustration.

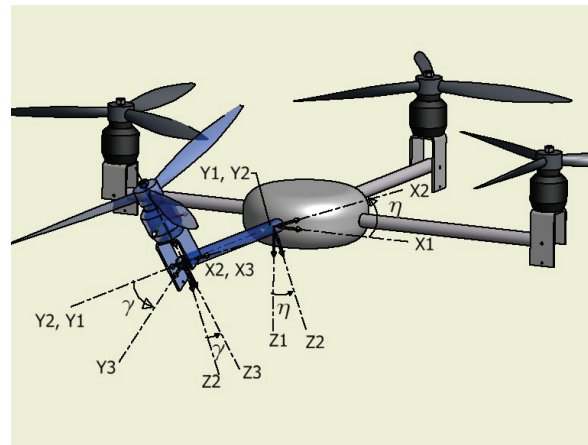


Figure 9. Reference frames used in the development. Note that  $\eta$  represents the servoblock angle and  $\gamma$  the pushpull angle.

The convention used to represents the different sets of unit vectors in the different reference frame is defined as follows. The vectors  ${}^i\mathbf{i}_j$ ,  ${}^i\mathbf{j}_j$ ,  ${}^i\mathbf{k}_j$  represent the unit vectors of reference frame  $j$  expressed in terms of the reference frame  $i$ .

Now in order to define the relationships between the different sets of unit vectors the rotation matrices between them must be stablished. The rotation matrix  $\mathbf{R}_{itoj}$  represents the relation between a vector  $\mathbf{v}$  expressed in reference frame  $i$ , i.e.  ${}^i\mathbf{v}$ , and a equivalent vector expressed in reference frame  $j$ , i.e.  ${}^j\mathbf{v}$ , such that:  ${}^j\mathbf{v} = \mathbf{R}_{itoj} {}^i\mathbf{v}$ .

From the geometry and the direction of the tilting motions illustrated in figure 9. The rotation matrices are defined as:

$$\mathbf{R}_{1to2} = \begin{bmatrix} \cos(\eta) & 0 & -\sin(\eta) \\ 0 & 1 & 0 \\ \sin(\eta) & 0 & \cos(\eta) \end{bmatrix} \text{ and } \mathbf{R}_{2to3} = \begin{bmatrix} 1 & 0 & 0 \\ 0 & \cos(\gamma) & \sin(\gamma) \\ 0 & -\sin(\gamma) & \cos(\gamma) \end{bmatrix} \quad (2)$$

where  $\eta$  is the servoblock angle and  $\gamma$  the pushpull angle. Since the rotation matrices are orthogonal their inverses are their transposes:

$$\mathbf{R}_{2to1} = \mathbf{R}_{1to2}^T \text{ and } \mathbf{R}_{3to2} = \mathbf{R}_{2to3}^T \quad (3)$$

Now the relations between the reference frames 1 and 3 can be established as:

$$\mathbf{R}_{1to3} = \mathbf{R}_{2to3} \mathbf{R}_{1to2} \text{ and } \mathbf{R}_{3to1} = \mathbf{R}_{2to1} \mathbf{R}_{3to2} \quad (4)$$

## 2. Rotor Inertia Definition

Figure 8(a) shows the rotating part of a thruster. It must be noted that since it has 3 blade propellers its mass distribution is the same regardless of the angle rotated. That is, it is symmetric with respect to the shaft. As a consequence, its inertia tensor around its CG with respect to a reference frame attached to the rotor and with the Z axis parallel to its shaft will be the same that if it is expressed with respect to a reference frame that is fixed in the stator of the motor, i.e. the swivelling bracket, as the reference frame 3 in figure 9.

The development of the Euler equation will be carried out exploiting this fact that the inertia tensor is constant if represented in the reference frame 3, i.e.  ${}^3\mathbf{I}$  is constant. Thus, in the Euler equation, eq 11, the motions,  $\boldsymbol{\alpha}$  and  $\boldsymbol{\omega}$ , must be expressed with respect to the reference frame 3, that is  ${}^3\boldsymbol{\alpha}_j$  and  ${}^3\boldsymbol{\omega}$ .

## 3. Motion Description

Now that the different relationships between the reference frames have been described the different motions affecting the spinning bodies can accurately defined with respect to the reference frame 3, i.e. that attached to the motor stator or the swivelling bracket.

The angular velocities undergone by the rotor will be the sum of the vehicle angular rates, i.e.  $p, q, r$ , the servo motion, i.e.  $\dot{\eta}$  and  $\dot{\gamma}$ , and the motor rotational speed  $\Omega$ .

$${}^3\boldsymbol{\omega} = \underbrace{{}^3\mathbf{i}_1 p + {}^3\mathbf{j}_1 q + {}^3\mathbf{k}_1 r}_{\text{Vehicle Motion}} + \underbrace{{}^3\mathbf{j}_1 \dot{\eta}}_{\text{servoblock}} + \underbrace{{}^3\mathbf{i}_2 \dot{\gamma}}_{\text{push pull}} + \underbrace{{}^3\mathbf{k}_3 \Omega}_{\text{Motor}} \quad (5)$$

Introducing the definitions of the unit vectors and the subsequent rotation matrices yields:

$${}^3\boldsymbol{\omega} = \begin{bmatrix} \cos(\eta)p - r \sin(\eta) + \dot{\gamma} \\ \sin(\gamma)(\cos(\eta)r + p \sin(\eta)) + \cos(\gamma)(q + \dot{\eta}) \\ \cos(\gamma)(\cos(\eta)r + p \sin(\eta)) + \Omega - \sin(\gamma)(q + \dot{\eta}) \end{bmatrix} \quad (6)$$

And the angular acceleration  ${}^3\boldsymbol{\alpha}$  is the time derivative of  ${}^3\boldsymbol{\omega}$ , hence:

$$\frac{d^3\omega}{dt} = {}^3\alpha = \begin{bmatrix} {}^3\alpha_X \\ {}^3\alpha_Y \\ {}^3\alpha_Z \end{bmatrix} \quad (7)$$

where:

$${}^3\alpha_X = \cos(\eta)\dot{p} - \sin(\eta)\dot{r} - (\cos(\eta)r + p \sin(\eta))\dot{\eta} + \Omega(\sin(\gamma)(\cos(\eta)r + p \sin(\eta)) + \cos(\gamma)(q + \dot{\eta})) + \ddot{\gamma} \quad (8)$$

$$\begin{aligned} {}^3\alpha_Y = & \cos(\gamma)\dot{q} + \sin(\gamma)(\sin(\eta)\dot{p} + \cos(\eta)\dot{r}) - \Omega(\cos(\eta)p - r \sin(\eta) + \dot{\gamma}) + \\ & \sin(\gamma)(\cos(\eta)p - r \sin(\eta))\dot{\eta} + \dot{\gamma}(\cos(\gamma)(\cos(\eta)r + p \sin(\eta)) - \sin(\gamma)(q + \dot{\eta})) + \cos(\gamma)\ddot{\eta} \end{aligned} \quad (9)$$

$$\begin{aligned} {}^3\alpha_Z = & -\sin(\gamma)\dot{q} + \cos(\gamma)(\sin(\eta)\dot{p} + \cos(\eta)\dot{r}) + \cos(\gamma)(\cos(\eta)p - r \sin(\eta))\dot{\eta} \\ & - \dot{\gamma}(\sin(\gamma)(\cos(\eta)r + p \sin(\eta)) + \cos(\gamma)(q + \dot{\eta})) + \dot{\Omega} - \sin(\gamma)\ddot{\eta} \end{aligned} \quad (10)$$

Now injecting the expressions of  ${}^3\omega$  and  ${}^3\alpha$  into the Euler equation, eq. 11, allows to calculate the moments that are applied onto the spinning assembly  ${}^3M$ :

$${}^3M = {}^3I^3\alpha + {}^3\omega \times {}^3I^3\omega \quad (11)$$

Since the interesting insight is the actions that the spinning assembly exerts onto the airframe the reactions referred to the vehicle frame, frame 1, shall be calculated. Hence, the moments that the spinning body applies onto the airframe in the reference frame of the vehicle,  ${}^1M_{Gyro}$ , are given by:

$${}^1M_{Gyro} = R_{3to1}(-{}^3M) = \begin{bmatrix} {}^3M_{React_X} \\ {}^3M_{React_Y} \\ {}^3M_{React_Z} \end{bmatrix} \quad (12)$$

where:

$$\begin{aligned} {}^1M_{Gyro_X} = & \frac{1}{4}(-2I_{xx}qr + I_{yy}qr + I_{zz}qr + 3I_{yy}\cos(2\gamma)qr - 3I_{zz}\cos(2\gamma)qr \\ & - 4I_{zz}\sin(\gamma)\Omega r + 2I_{yy}\dot{\eta}r + 2I_{zz}\dot{\eta}r + 2I_{yy}\cos(2\gamma)\dot{\eta}r - 2I_{zz}\cos(2\gamma)\dot{\eta}r - 2I_{xx}\dot{p} - I_{yy}\dot{p} \\ & - I_{zz}\dot{p} + I_{yy}\cos(2\gamma)\dot{p} - I_{zz}\cos(2\gamma)\dot{p} - 2I_{yy}p\sin(2\gamma)\dot{\gamma} + 2I_{zz}p\sin(2\gamma)\dot{\gamma} \\ & - \sin(2\eta)(4(I_{xx} - I_{yy})p\sin(\gamma)\Omega + 2(I_{yy} - I_{zz})r\sin(2\gamma)\dot{\gamma} - (2I_{xx} - I_{yy} - I_{zz})(\dot{r} + p(q + 2\dot{\eta})) \\ & - (I_{yy} - I_{zz})\cos(2\gamma)(\dot{r} + p(q + 2\dot{\eta}))) - \cos(2\eta)(4(I_{xx} - I_{yy})r\sin(\gamma)\Omega + 2(I_{zz} - I_{yy})p\sin(2\gamma)\dot{\gamma} \\ & + (2I_{xx} - I_{yy} - I_{zz})(\dot{p} - r(q + 2\dot{\eta})) + (I_{yy} - I_{zz})\cos(2\gamma)(\dot{p} - r(q + 2\dot{\eta}))) \\ & - 2\cos(\eta)(2(I_{xx} - I_{yy} + I_{zz})\cos(\gamma)\Omega(q + \dot{\eta}) + (I_{yy} - I_{zz})\sin(2\gamma)(q - r + \dot{\eta})(q + r + \dot{\eta}) + 2I_{xx}\ddot{\gamma} \\ & - 2\sin(\eta)(-2(-I_{xx} + I_{yy} + I_{zz})\sin(\gamma)\Omega\dot{\gamma} - 2I_{xx}(q + \dot{\eta})\dot{\gamma} + \\ & 2(I_{yy} - I_{zz})\cos(2\gamma)(q + \dot{\eta})\dot{\gamma} + 2I_{zz}\cos(\gamma)\dot{\Omega} - (I_{yy} - I_{zz})\sin(2\gamma)(pr - \dot{q} - \ddot{\eta}))) \end{aligned} \quad (13)$$

$$\begin{aligned} {}^1M_{Gyro_Y} = & \frac{1}{4}(-2I_{xx}\sin(2\eta)p^2 + I_{yy}\sin(2\eta)p^2 + I_{zz}\sin(2\eta)p^2 - 4I_{xx}\cos(2\eta)rp \\ & + 2I_{yy}\cos(2\eta)rp + 2I_{zz}\cos(2\eta)rp - 4I_{xx}\sin(\eta)\dot{\gamma}p + 2I_{xx}r^2\sin(2\eta) - \\ & I_{yy}r^2\sin(2\eta) - I_{zz}r^2\sin(2\eta) - 2I_{yy}\dot{q} - 2I_{zz}\dot{q} - 4I_{xx}\cos(\eta)r\dot{\gamma} - 4(I_{xx} - I_{yy} - I_{zz})\cos(\gamma)\Omega(\cos(\eta)p \\ & - r\sin(\eta) + \dot{\gamma}) + 2(I_{yy} - I_{zz})\sin(2\gamma)(-\sin(\eta)(qr + \dot{p}) + \cos(\eta)(pq - \dot{r}) + 2\dot{\gamma}(q + \dot{\eta})) + 4I_{zz}\sin(\gamma) \\ & \dot{\Omega} - 2I_{yy}\ddot{\eta} - 2I_{zz}\ddot{\eta} - 2(I_{yy} - I_{zz})\cos(2\gamma)(\dot{q} + (\cos(\eta)r + p \sin(\eta))(\cos(\eta)p - r \sin(\eta) + 2\dot{\gamma}) + \ddot{\eta})) \end{aligned} \quad (14)$$

$$\begin{aligned}
{}^1\mathbf{M}_{\text{Gyro}_Z} = & \frac{1}{4}(-2(I_{yy} - I_{zz}) \sin(2\gamma) \sin(\eta)p^2 - (4(I_{yy} - I_{zz}) \cos(2\gamma)\dot{\eta} \sin^2(\eta) \\
& + (2(-2I_{xx} + I_{yy} + I_{zz}) \cos^2(\eta) - (I_{yy} - I_{zz}) \cos(2\gamma)(\cos(2\eta) - 3))q \\
& - 4(I_{zz} + (I_{yy} - I_{xx}) \cos(2\eta)) \sin(\gamma)\Omega + 2(I_{yy} - I_{zz}) \cos(\eta) \sin(2\gamma)(r + 2 \sin(\eta)\dot{\gamma}) + \\
& 2(I_{yy} + I_{zz} + (-2I_{xx} + I_{yy} + I_{zz}) \cos(2\eta))\dot{\eta}p - 2I_{xx}\dot{r} - I_{yy}\dot{r} - I_{zz}\dot{r} + I_{yy} \cos(2\gamma) \\
& \dot{r} - I_{zz} \cos(2\gamma)\dot{r} - 2I_{yy}r \sin(2\gamma)\dot{\gamma} + 2I_{zz}r \sin(2\gamma)\dot{\gamma} - \cos(2\eta)((-2I_{xx} + I_{yy} + I_{zz} + (I_{zz} - I_{yy}) \cos(2\gamma))\dot{r} + \\
& 2(I_{yy} - I_{zz})r \sin(2\gamma)\dot{\gamma} - \sin(2\eta)(4(I_{yy} - I_{xx})r \sin(\gamma)\Omega + (2I_{xx} - I_{yy} - I_{zz})(r(q + 2\dot{\eta}) - \dot{p}) \\
& + (I_{yy} - I_{zz}) \cos(2\gamma)(r(q + 2\dot{\eta}) - \dot{p})) - 2 \sin(\eta)(-(I_{yy} - I_{zz}) \sin(2\gamma)(q + \dot{\eta})^2 \\
& - 2(I_{xx} - I_{yy} + I_{zz}) \cos(\gamma)\Omega(q + \dot{\eta}) - 2I_{xx}\ddot{\gamma}) - 2 \cos(\eta)(-2(-I_{xx} + I_{yy} + I_{zz}) \sin(\gamma)\Omega\dot{\gamma} \\
& - 2I_{xx}(q + \dot{\eta})\dot{\gamma} + 2(I_{yy} - I_{zz}) \cos(2\gamma)(q + \dot{\eta})\dot{\gamma} + 2I_{zz} \cos(\gamma)\dot{\Omega} + (I_{yy} - I_{zz}) \sin(2\gamma)(\dot{q} + \dot{\eta})))
\end{aligned} \tag{15}$$

### C. Propeller Characterisation

Usually, in the literature of quadrotor design, analytical calculations are conducted to obtain the Thrust and Torque coefficients of the propellers, see<sup>3</sup>. These calculations are mostly based on Blade Element Theory and Momentum theory. Also, another alternative would be to use Goldstein's Vortex Theory of Screw Propellers, see<sup>19</sup>. All these methods require more or less an extensive geometric description of the propeller. Since the manufacturer was not able to provide this information, and because measuring it was a challenge in itself, it was decided instead to measure experimentally the propeller characteristics. Since the initial model was to design a controller around hover or quasi hover, no advance nor vertical velocity was considered. Hence, the measurements were performed in a static rig for both Thrust and Torque across all the range of attainable rpm regimes.

The rig used for the measurements of torque and thrust is shown in figures 10(a) and 10(b) respectively. The angular speed of the propeller was measured by means of a laser beam and phototransistor setup shown in figure 10(c). The main advantage of the laser setup compared to a traditional handheld tachometer is that it allows for dynamic measurements, something that will prove useful in the next section.

Using the definitions for the Thrust and Torque coefficient given by Leishman<sup>10</sup>:

$$T = \rho A(\Omega R)^2 C_T \text{ and } Q = \rho A(\Omega R)^2 R C_Q \tag{16}$$

the thrust and torque coefficients are found from fitting the slopes to the experimental data as shown in figures 11(a) and 11(b), with  $C_T = 0.013$  and  $C_Q = 0.0013$ .

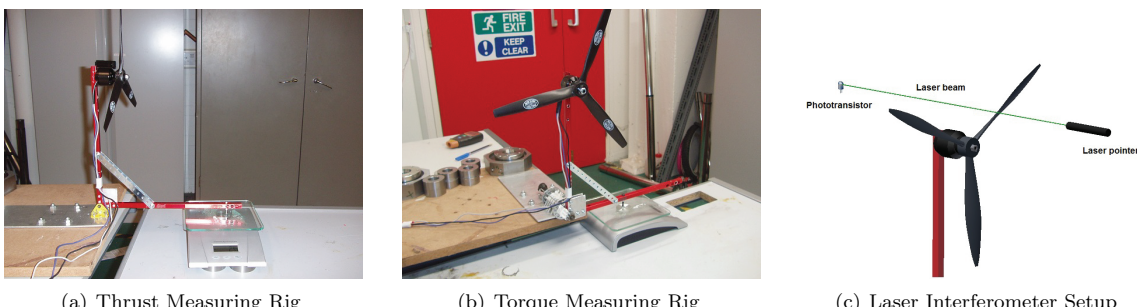
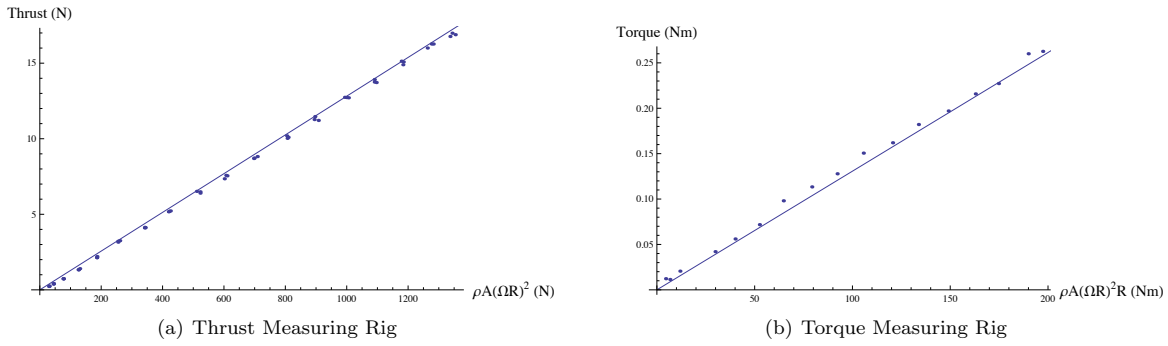


Figure 10. Spinning body and arm numbering illustration.



**Figure 11.** Slope fitting for aerodynamic coefficient obtention.

#### D. Actuator Characterisation

In order to simulate effectively the vehicle's dynamics, it is fundamental to have an accurate model of the dynamics of its main control action generators, that is, the motors and the servomotors. To achieve this, a series of experiments were conducted to gather information about the system behaviour. The modelling of the actuators is broken in three parts, the motors, the servoblock servomotors and the push-pull servomotors.

To reduce the model complexity and uncertainty that would have resulted from an attempt to model each of the individual systems from physical principles, a pragmatic black-box approach was undertaken, where the relationship between input commands and outputs the whole system was abstracted into a single transfer function for each of the actuators that was found from empirical data.

The approach followed for the identification of the system dynamics in the three cases was to feed sinusoidal commands around a nominal point with different frequencies and, then, to record the phase and amplitude of the output. Thus, allowing to get a clear picture of the gain and the phase lag of the system at each given frequency. Once a representative set of points describing the frequency response was obtained a transfer function was identified by fitting a combination of primitive transfer functions such as first and second order and a time delay.

##### 1. Motors

To characterise the dynamics of the motor a transfer function from throttle input in (%) to angular velocity (rad/s) output was identified. Both parameters, throttle and angular velocity of the propeller, are defined as increments around the operating point defined by a nominal thrust of 7.5N, i.e. 3kg of all up mass. These parameters depend strongly upon the whole propulsive system that is: the motor itself, the speed controller and the propeller. Hence the transfer function represents a lumped model of all the combination of the effects of all the different systems. To do this, as mentioned before, a series of sinusoidal throttle commands were fed into the system and recorded whilst the response of the angular velocity was accurately measured at each blade pass by a laser phototransistor shown in figure 10(c). Hence, by estimating the gain and phase of both the input and the output at different frequencies a bode plot can be constructed, upon which a transfer function can be fitted. In this case, the system is represented by a 1st order system with a delay. In figure 13(a) the test data is shown alongside the identified system, the transfer function found is,  $G_{\text{Motor}}$ , given by:

$$G_{\text{Motor}} = \frac{\text{Angular Velocity}}{\text{Throttle Input}} = \frac{\Delta\omega (\frac{\text{rad}}{\text{s}})}{\Delta\tau (0 \text{ to } 1)} = \frac{e^{-0.035s} 9.19}{(1 + 0.16s)} \quad (17)$$

##### 2. Servomotors

A servomotor is a device that receives an angle as input encoded in a PWM signal and moves its lever to the position requested. They are widely used in the RC hobby market due to their compact size, ease of use, simplicity and low weight compared to traditional DC motor and driving circuitry.

On the other hand, their dynamics are not trivial; since they implement an internal controller to regulate their position, their input and output are thus position. The whole servomotor is composed essentially by a DC motor with gearbox, a potentiometer and a driver circuit with a controller.

In the vehicle, servomotors are used to drive both the servo block mechanism and the push pull mechanism, the servo used is the HS-7940TH. Although all the servos are exactly the same they drive different inertias at different gearing ratios, so a full model of the arm was constructed to independently produce the system identification data. See figure 12(a) for the illustration of the servoblock motion and figure 12(b) for the push-pull motion.

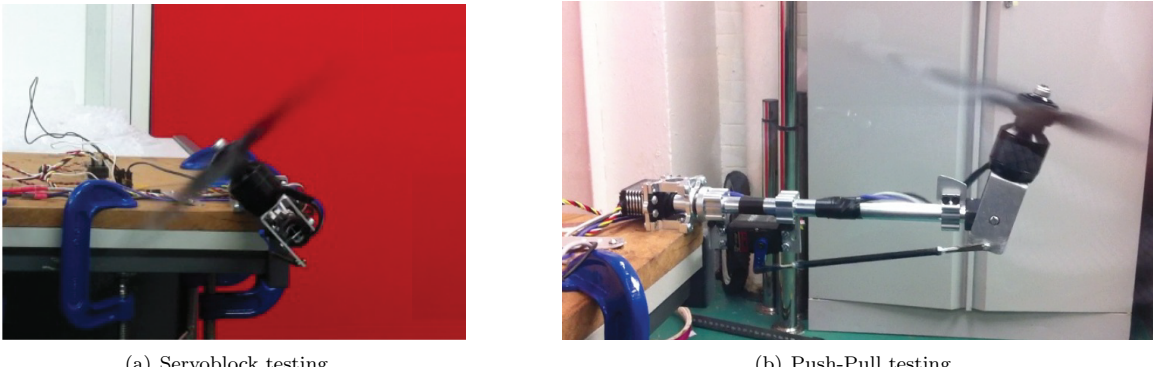


**Figure 12. Testing of the servomotors on the prototype arm.**

The accuracy of this model is critical because, as can be seen in the Gyroscopic Effects Modelling section, an important control action depends upon the angular rates  $\dot{\eta}$  and  $\dot{\gamma}$ . Therefore the control system design will be dependant on whether the model represents faithfully the reality. Hence, because  $\dot{\eta}$  and  $\dot{\gamma}$  are given by the dynamics of the servomotor response is critical to the success of the modelling to obtain a representative estimate of its transfer function.

In practice the angle of the servo can not be measured easily but it can be modified to fit a wire to read its internal potentiometer. Then, a mapping between the voltage of the potentiometer and the angle is conducted. These mappings resulted in the acquisition of the gains to relate both, PWM mS to requested angle and potentiometer voltage reading to the actual angle.

The operating voltage for the servos is 7.4V, hence, all the tests have been conducted feeding a nominal 7.4V from a power supply to the servos. To simulate conditions about the nominal point, the propeller was running at nominal rpm that is around 5000 rpm which corresponds to a nominal thrust of 7.5N.

As with the motor system identification a usb oscilloscope was set up to read the input PWM signal sent to the servo and the output in this case the voltage of the internal potentiometer. The strategy followed in the feeding of the signals was the same as with the motor, that is, several sinusoids were fed over a range of relevant frequencies and the amplitude and phase were obtained.

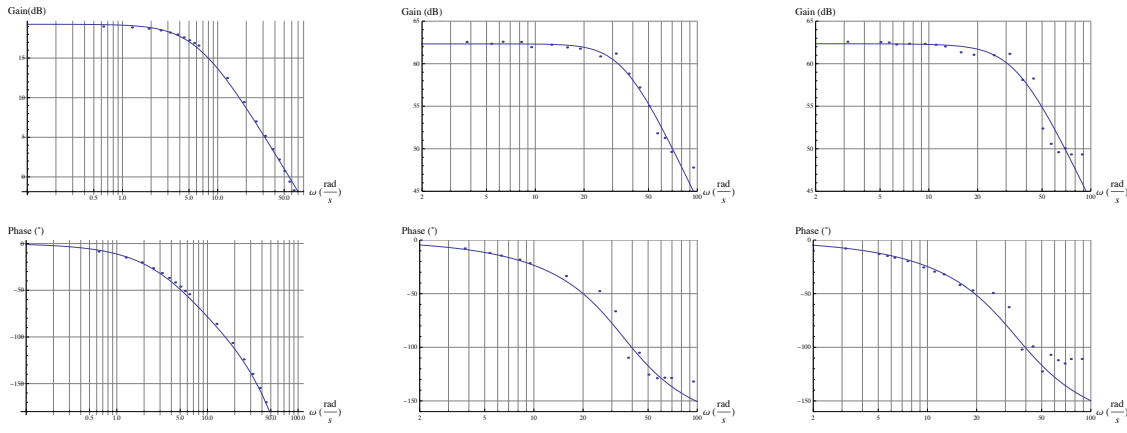
It can be seen in figures 13(b) and 13(c), that, for both servoblock and pushpull servos, the gain shows a negative slope of about -40dB per decade, therefore, a second order system is chosen to represent its dynamic behaviour. With a least squares method between the experimental data and the function in both in dB, the parameters of the function were found yielding the transfer functions:

$$G_{\text{servoblock}} = \frac{\text{Actual Angle}}{\text{Requested Angle}} = \frac{\eta \text{ (rad)}}{\eta_{\text{Requested}} \text{ (rad)}} = \frac{1228.05}{1228.05 + 49.18s + s^2} \quad (18)$$

$$G_{\text{pushpull}} = \frac{\text{Actual Angle}}{\text{Requested Angle}} = \frac{\gamma \text{ (rad)}}{\gamma_{\text{Requested}} \text{ (rad)}} = \frac{1212.73}{1212.73 + 51.11s + s^2} \quad (19)$$

### E. Thrusting Torques

The thrusters have two main sources of aerodynamic torques. One is the torque created by the thrust and the other is the drag torque. Again for arm 3 they can be expressed as:



(a) **Motor** frequency response, experimental data and fitted transfer function  $G_{\text{motor}}$  (note gain is  $\frac{\text{Angular Velocity}}{\text{Throttle Input}} = \frac{\Delta\omega (\text{rad/s})}{\Delta\tau (0 \text{ to } 1)}$  ).

(b) **Servoblock** frequency response, experimental data and fitted transfer function  $G_{\text{Servoblock}}$  (note gain is  $\frac{\text{Feedback Volts}}{\text{Pulse Uptime}} = \frac{\Delta V \text{ Volts}}{\Delta t (\text{S})}$  ).

(c) **Push-Pull** frequency response, experimental data and fitted transfer function  $G_{\text{Push-Pull}}$  ( $\frac{\text{Feedback Volts}}{\text{Pulse Uptime}} = \frac{\Delta V \text{ Volts}}{\Delta t (\text{S})}$  ).

**Figure 13. Frequency responses, experimental data and fitted transfer functions.**

$$\mathbf{M}_{\text{Motor}_3} = \mathbf{r}_{\text{Hub2CG}} \times \mathbf{T}_{\text{Motor}} + \mathbf{Q} = T \begin{bmatrix} L \cos(\gamma) \cos(\eta) - H \sin(\gamma) \\ -H \cos(\gamma) \sin(\eta) \\ -L \cos(\gamma) \sin(\eta) \end{bmatrix} + Q \begin{bmatrix} \cos(\gamma) \sin(\eta) \\ -\sin(\gamma) \\ \cos(\gamma) \cos(\eta) \end{bmatrix} \quad (20)$$

For the remaining arms the torque is easily calculated by projection, hence, the total aerodynamic moment on the vehicle is:

$$\mathbf{M}_{\text{MotorTotal}} = \sum_{j=1}^4 \mathbf{R}_{3toj} \mathbf{M}_{\text{Motor}_3} \quad (21)$$

## F. Equations of motion

The equations of motion used in the development of the model are the standard full 6 degree of freedom for a rigid aircraft. Its development can be found in any book about Flight Dynamics, the interested reader can refer, for example, to Cook<sup>4</sup> or Stengel<sup>17</sup>.

$$\begin{cases} X = m(\dot{u} + qw - rv) \\ Y = m(\dot{v} + ru - pw) \\ Z = m(\dot{w} + pv - qu) \\ L = I_x \dot{p} - I_{yz}(r^2 - p^2) - I_{xy}(\dot{p} + pq) - I_{xy}(\dot{q} - rp) - (I_y - I_z)qr \\ M = I_y \dot{q} - I_{zx}(r^2 - p^2) - I_{xy}(\dot{p} + qr) - I_{yz}(\dot{r} - pq) - (I_z - I_x)rp \\ Z = I_z \dot{r} - I_{xy}(p^2 - q^2) - I_{yz}(\dot{q} + rp) - I_{zx}(\dot{p} - qr) - (I_x - I_y)pq \end{cases} \quad (22)$$

For the representation of the angles, the Euler formulation was chosen, therefore, the Euler angular rates were given, as a function of p, q and r by:

$$\begin{bmatrix} \dot{\phi} \\ \dot{\theta} \\ \dot{\psi} \end{bmatrix} = \begin{bmatrix} 1 & \sin \phi \tan \theta & \cos \phi \tan \theta \\ 0 & \cos \phi & -\sin \phi \\ 0 & \frac{\sin \phi}{\cos \theta} & \frac{\cos \phi}{\cos \theta} \end{bmatrix} \begin{bmatrix} p \\ q \\ r \end{bmatrix} \quad (23)$$

## G. Simulation Model

### 1. Main Structure

All these modelling equations were implemented in the simulation model. The main structure of the simulation model can be seen in figure 14. It is composed of 4 main blocks:

- **Controller:** From the sensor reading, it issues the virtual control commands.
- **Control Allocator:** This block contains the logic that distributes the virtual input demands into the individual control inputs.
- **Vehicle Dynamics:** Contains the actuator equations and the equations of motion that have been developed in this section. The internal workings of this block will be further developed.
- **Sensor (IMU):** Represents the sensor suite, in this case it simulates the IMU and the inherent noise.

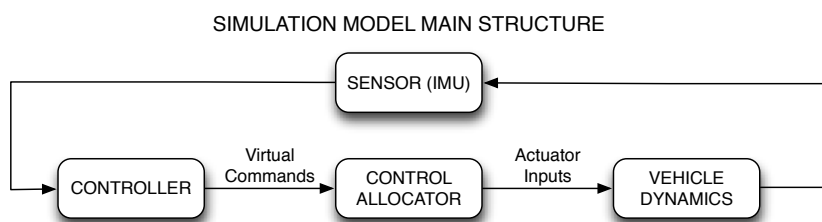


**Figure 14. Main structure of the simulation model.**

### 2. Vehicle Dynamics Block

In figure 15 the inside of the vehicle dynamics block is shown, this block contains the motion of the vehicle and the actions exerted onto it. It is composed by:

- **Actuator:** Contains the action of the individual arms, both aerodynamic and rigid body. Its inputs are both the rotation motion of the vehicle and the control inputs.
- **Gravity:** Generates the gravitational forces and projects it into body axis. In this case there are no moments since the EOM are centered in the CG.
- **Perturbation:** Contains the terms to generate perturbations to test the controllers.
- **6DOF Equations of Motion:** Is composed of the 6DOF equations of motion described in this section: equations 22 and 23. These equations are centred in the CG, therefore all forces and moments which are inputted to it have to be transported to the CG.

### 3. Actuators Block

The actuators block, see figure 16, is composed of the four arms of the vehicle. Each of them generates forces and moments according to the control inputs and according to the rotation of the vehicle. The inside of each of the blocks is the same, and implements all the dynamics and aerodynamics developed in this section. The only change on each arm block is the projection of the axis to account for the position of each individual arm. Note that the layout of the arms is the same as in the vehicle, Arm 1 is the front, 2 the back, 3 the right and 4 the left.

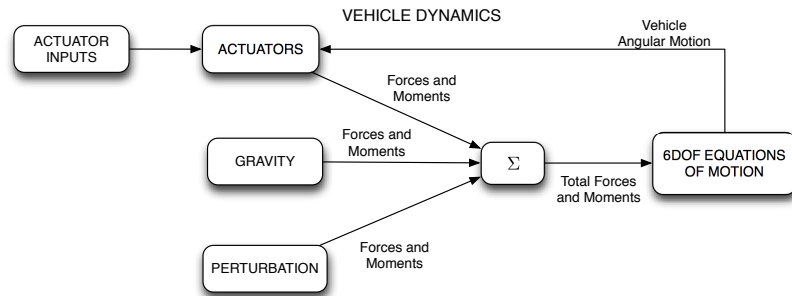


**Figure 15. Inside of the Vehicle Dynamics Block.**

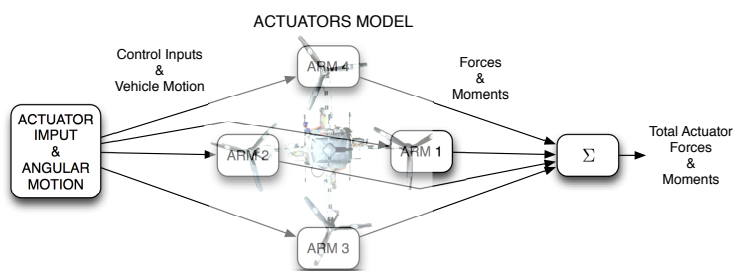


**Figure 16. Actuator Block, generates the forces and moments from the control inputs and the angular motion.**

#### 4. Standard Actuator Block

The Standard Actuator block, see figure 17, is the block that mechanises all the equations developed in this section. The approach followed was to project calculate the forces and moments for a Standard Arm, that is, the one described in the Rigid Body section and then rotate the forces and moment vectors according to each individual arms.

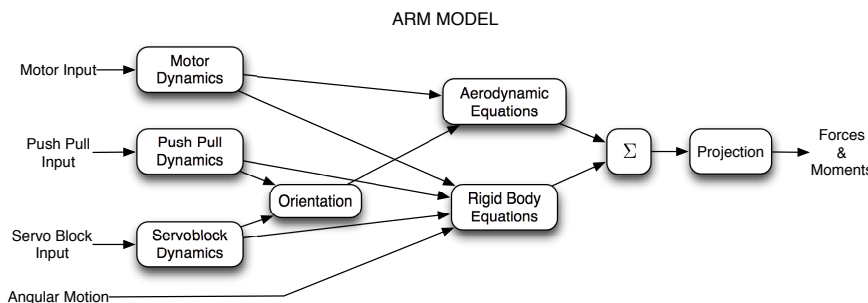


**Figure 17. Standard Actuator model, mechanises the dynamics: Rigid Body and Aerodynamics of an arm.**

First there is the individual actuators dynamics which creates the motion that is fed to the aerodynamic equations and the rigid body equations. They are:

- **Motor Dynamics:** Reads the control input for the motor and outputs the angular velocity,  $\Omega$ , and angular acceleration,  $\dot{\Omega}$ , of the rotation assembly. According to the dynamics developed, equation 17. If the propeller in this arm is rotating anticlockwise from above then it outputs the negated angular velocity:  $-\Omega$ , and angular acceleration:  $-\dot{\Omega}$ .
- **Push Pull Dynamics:** Reads the control input to the Push Pull and through the Push Pull dynamics developed, (equation 19) outputs the angle  $\gamma$ , the angular velocity  $\dot{\gamma}$  and the angular acceleration  $\ddot{\gamma}$ .
- **Servo Block Dynamics:** From the input to the Servoblock servo generates the angle  $\eta$ , angular velocity  $\dot{\eta}$  and angular acceleration  $\ddot{\eta}$  using the transfer function developed, (equation 18).

The Aerodynamic and Rigid Body blocks take the motion of the individual actuator, Motor, Push Pull and Servoblock and calculate the Forces and Moments that they create. That is thrust and its torque in the CG, drag torque, and the gyroscopic or rigid body moments. Its blocks are:

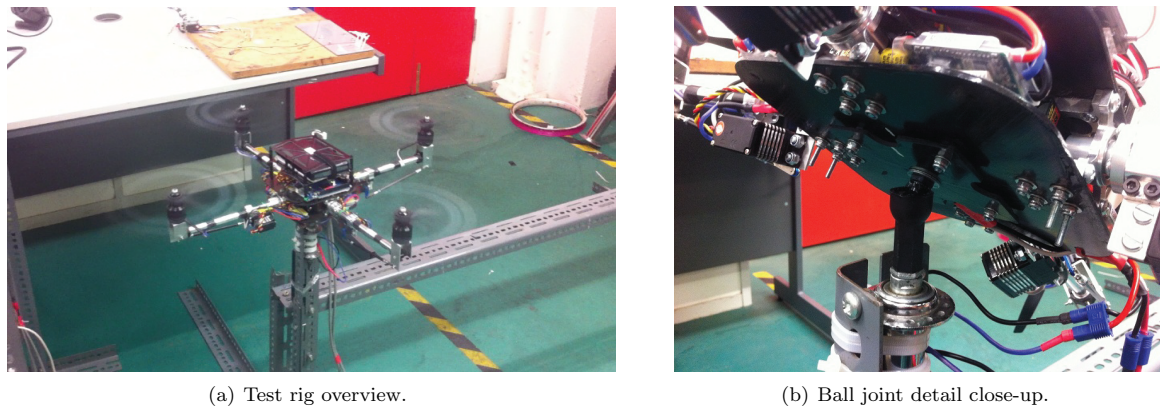
- **Aerodynamic Block:** This block generates the thrust(equation 16), the moment that the thrust generates around the CG and the drag torque (equation 16) from the spinning propeller motion  $\Omega$ . It does so from the equations derived in the aerodynamic section taking into account the orientation of the tilted propeller, i.e.,  $\eta$  and  $\gamma$ .
- **Rigid Body Block:** Mechanises the equations derived in the Rigid Body section (equation 12). That is, it generates the gyroscopic (Rigid Body) moments from the rotating propeller motion  $\Omega$   $\dot{\Omega}$ , the angular motion of the body,  $p$   $q$   $r$   $\dot{p}$   $\dot{q}$   $\dot{r}$ , the motion of the servoblock  $\eta$   $\dot{\eta}$   $\ddot{\eta}$  and the motion of the pushpull  $\gamma$   $\dot{\gamma}$   $\ddot{\gamma}$ .

Once the Forces and Moments have been computed around the CG in body axis created by the Standard Arm, they have to be projected in each of the four individual arms. To clarify this as an example let's see the difference between Arm 1 and 2. They both create the same forces and moments when they are fed the same control inputs or the same vehicle motion, but the axis of its components is different with respect to the body axis. So the magnitude of the forces and moments is the same, the only difference is in the directions. Hence, there is no need to re-derive all the rigid body equations as it can simply be rotated accordingly to the position of each arm. This is dealt with by the projection block.

## V. Test and Validation

### A. Experimental Setup

During the development process a bench was pourposely built in order to check the correct function of the systems, to validate the simulation model and to tune the controller. This bench allowed for the freedom of the 3 angles, roll, pitch and yaw and only constrained the position at the joint. A picture of it is shown in figures 18(a) and 18(b). The power was supplied via an external power supply in order to maintain always the same nominal voltage. For the details on the setup see the theses by Al-Rihani<sup>2</sup> and Segui-Gasco<sup>6</sup>.



(a) Test rig overview.

(b) Ball joint detail close-up.

**Figure 18. Detail of the ball joint rig.** The ball joint is attached to a frame by a bicycle hub that allows the ball joint to spin, yaw, freely. On its side, the ball joint allows for free movement of the pitch and roll motions. Hence, the only motion constrained is the translational.

While the rig itself is very useful to conduct tests in near flight conditions, there are, several effects that make its dynamics differ from the actual flight condition. One of the most significant is the torque created by the offset of the reaction forces exerted by the joint and the CG. Thus, to make an appropriate comparison an additional force term hast o be added to the simulation.

The nature of this effect is very de-stabilising because it adds a component that tends to pull out the vehicle from the equilibrium point, it can be thought as an inverted pendulum, with the addition of the thrust that since it is projected, it adds to large de stabilising torque. Hence, the response will be more oscillatory and will overshoot much more than in actual flight.

To model the reaction torque, the forces and moments that it creates onto the vehicle have to be analysed. Basically, the force that the joint exerts onto the vehicle is the reaction to the resultant of the forces that are applied onto the airframe, namely thrust and weight. Hence, the moment that the joint creates is the resultant of the transport of the aforementioned reaction force to the CG, i.e.  $\mathbf{M}_{\text{Joint}} = \mathbf{r}_{\text{CG2Joint}} \times \mathbf{F}_{\text{Resultant}}$ . Hence, to include the dynamics of the ball joint the following actions have to be included into the simulation model:

$$\mathbf{F}_{\text{Joint}} = -\mathbf{F}_{\text{Resultant}} = -\Sigma \mathbf{F} \quad \mathbf{M}_{\text{Joint}} = \mathbf{r}_{\text{CG2Joint}} \times \mathbf{F}_{\text{Joint}} \quad (24)$$

With this modifications, the simulation model is, then, comparable with the experimental results from the ball joint test rig. In the following the results of the simulation are to be compared with the ball joint test rig for the different axes, Roll, Pitch and Yaw, to assess the accuracy of the modelling.

### B. Simulation Validation

To get a good picture of the dynamics of the system, specially, of the high frequency components which contain the most uncertainty, it was thought that the best benchmark signal would be an impulse. Ideally this comparison should have been with the open loop system, however due to inherent instability of the system and its complexity, 12 control inputs, as a first rough comparison, a closed loop system comparison was carried out. Thus, the time histories presented of the simulation include the effect of the control system, this was done by putting in the simulation model the exact same gains as in the vehicle and including the

processing and communications delay measured between the sensor to the controller and to the individual actuators. To generate the time histories in the test rig, with the transmitter stick an impulse was created and both the response of the real vehicle and the input were recorded. Then, the recorded command was fed into the simulation model and the response are compared for all three axes.

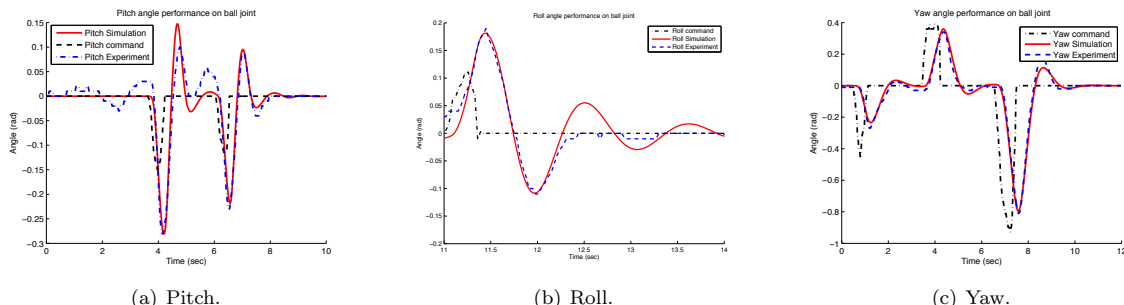


**Figure 19.** Comparison of the simulation response and the experiments in the ball joint rig. Note the overshooting tendency due to the inverted pendulum effect created by offset of the ball joint and the CG.

### Pitch

In figure 19(a) the response to an impulse from the transmitter is represented for both the simulation and the vehicle in the ball joint. It can be seen that although the signal quantisation does not allow for much resolution, the trend in the amplitudes of the peaks and the frequency are very similar to each other. The existence of overshoot and the underdamping tendency is due inverted pendulum like de-stabilising action of the ball joint rig to real vehicle. According to the simulation, in flight the vehicle does not experience this kind of underdamped dynamics.

### Roll

Similarly to the Pitch, the Roll comparison in figure 19(b) shows a very similar frequency. Regarding the damping, the ratios of the amplitudes appear to be very close one to another, but, the quantisation of the experimental signal, again, does not allow for a precise conclusion. Similarly with the pitch, the existence of overshoot and the underdamping tendency is due to the de-stabilising effect introduced by the rig moments. Again, according to the simulation, in flight the vehicle does not experience this kind of underdamped dynamics.

### Yaw

To assess the performance in the yaw axis of the simulation model, a train of pulses were sent to the vehicle and the response was recorded and the same pulses were fed into de simulation model. The result is plot in figure 19(c). It can, then, be seen that the model represents with fidelity the behaviour of the real vehicle since the amplitudes of the peaks are almost the same, indicating similar damping, and the time between peaks is also very similar, thus, indicating the similar frequency.

## VI. Analysis and Discussion

Evidence has been presented that the overall the simulation model qualitatively follows the trends of the real vehicle with fidelity. This is only a first step in the validation of the model and a more extensive quantitative validation based on flight test data should be carried out in the future. Also a series of open loop tests could be carried out to identify the effect of each individual actuator, this could be done by constructing some kind of dynamical measurement system of the torques, in order to further increase the confidence of the simulation model results.

In this paper a presentation of the design of a novel quadrotor platform has been carried out. This new concept implements a dual axes tilting propellers that are used to generate actuation forces and moments, these are produced through 3 main mechanisms, gyroscopic torques, thrust vectoring and differential thrusting. In order to produce a simulation model of this vehicle a careful analysis of the system dynamics has been carried out. First, a derivation of the rigid body equation for the tilting propellers is presented. Second, the propellers are empirically characterised through its thrust and torque coefficients. Third, and finally, a series of experiments are presented in order to obtain a transfer function to model the motors dynamics, both the thrusters and the servomotors. All this relations are put together in the form of a simulation model which is satisfactorily validated against experiments with the whole vehicle on a test rig.

## References

- <sup>1</sup>O. Garcia A. Sanchez, J. Escareño and R. Lozano. Autonomous hovering of a noncyclic tiltrotor uav: Modeling, control and implementation. *Proceedings of the 17th World Congress The International Federation of Automatic Control. Seoul, Korea.*, July 2008.
- <sup>2</sup>Yazan Al-Rihani. Development of a dual axis tilt rotorcraft uav: Design, prototyping and control. *MSc Thesis, Cranfield University*, 2012.
- <sup>3</sup>Samir Bouabdallah. *Design and control of quadrotors with application to autonomous flying*. PhD thesis, 2007.
- <sup>4</sup>Michael V. Cook. *Flight Dynamic Principles*. Elsevier/Butterworth-Heinemann, 2007.
- <sup>5</sup>Mark Cutler, Nazim-Kemal Ure, Bernard Michini, and Jonathan How. *Comparison of Fixed and Variable Pitch Actuators for Agile Quadrotors*. American Institute of Aeronautics and Astronautics, 2013/01/14 2011.
- <sup>6</sup>Pau Seguí Gascó. Development of a dual axis tilt rotorcraft uav: Modelling, simulation and control. Master's thesis, Cranfield University, 2012.
- <sup>7</sup>G. R. Gress. Using dual propellers as gyroscopes for tilt- prop hover control. *Proc. AIAA Biennial Int. Powered Lift Conf. Exhibit, Williamsburg, VA*, Nov. 2002.
- <sup>8</sup>Gary R. Gress. Lift fans as gyroscopes for controlling compact vtol air vehicles: Overview and development status of oblique active tilting. *American Helicopter Society 63th Annual Forum, Virginia Beach, VA*, May 2007.
- <sup>9</sup>F. Kendoul, I. Fantoni, and R. Lozano. Modeling and control of a small autonomous aircraft having two tilting rotors. In *Decision and Control, 2005 and 2005 European Control Conference. CDC-ECC '05. 44th IEEE Conference on*, pages 8144 – 8149, dec. 2005.
- <sup>10</sup>J.G. Leishman. *Principles of Helicopter Aerodynamics*. Cambridge Aerospace Series. Cambridge University Press, 2006.
- <sup>11</sup>Y-Y.; Moerder D. D.; Cooper E. G Lim, K. B.; Shin. A new approach to attitude stability and control for low airspeed vehicles. *AIAA Guidance, Navigation and Control Conference and Exhibit; ; Providence, RI; United States*, 16-19 Aug. 2004.
- <sup>12</sup>Chang How Lo, Hyo-Sang Shin, Antonios Tsourdos, and Seungkeun Kim. *Modeling and Simulation of Fault Tolerant Strategies for A Quad Rotor UAV*. American Institute of Aeronautics and Astronautics, 2013/01/14 2012.
- <sup>13</sup>R. Mahony, V. Kumar, and P. Corke. Multirotor aerial vehicles: Modeling, estimation, and control of quadrotor. *Robotics Automation Magazine, IEEE*, 19(3):20 –32, sept. 2012.
- <sup>14</sup>R. Davies N. Amiri, A. Ramirez-Serrano. Modelling of opposed lateral and longitudinal tilting dual-fan unmanned aerial vehicle. *18th IFAC World Congress Milano (Italy)*, Sept. 2011.
- <sup>15</sup>P. Segui-Gasco, Y. Al-Rihani, H. Shin, and A. Savvaris. Novel actuation concept for a multi rotor uav. *International Conference on Unmanned Aircraft Systems, ICUAS, (To Appear)*, 2013.
- <sup>16</sup>ServoCity. <http://www.servocity.com/>, may 2012.
- <sup>17</sup>F. Robert Stengel. *Flight Dynamics*. Princeton University Press, 2004.
- <sup>18</sup>Ryohei Kitayoshi Ichiro Maruta Toshiharu Sugie Takashi Wada, Masato Ishikawa. Practical modeling and system identification of r/c servo motors. *18th IEEE International Conference on Control Applications Part of 2009 IEEE Multi-conference on Systems and Control Saint Petersburg*, July 8-10, 2009.
- <sup>19</sup>Quentin R. Wald. The aerodynamics of propellers. *Progress in Aerospace Sciences*, 42(2):85 – 128, 2006.